

Article

Impact of Solid-State Charge Injection on Spectral Photoresponse of NiO/Ga₂O₃ p–n Heterojunction

Alfons Schulte ^{1,2,*} , Sushrut Modak ¹ , Yander Landa ¹, Atman Atman ¹, Jian-Sian Li ³ ,
Chao-Ching Chiang ³ , Fan Ren ³ , Stephen J. Pearton ⁴  and Leonid Chernyak ^{1,*}

¹ Department of Physics, University of Central Florida, Orlando, FL 32816, USA

² College of Optics and Photonics, University of Central Florida, Orlando, FL 32816, USA

³ Department of Chemical Engineering, University of Florida, Gainesville, FL 32611, USA

⁴ Material Science and Engineering, University of Florida, Gainesville, FL 32611, USA

* Correspondence: alfons.schulte@ucf.edu (A.S.); leonid.chernyak@ucf.edu (L.C.)

Abstract: Forward bias hole injection from 10-nm-thick p-type nickel oxide layers into 10- μ m-thick n-type gallium oxide in a vertical NiO/Ga₂O₃ p–n heterojunction leads to enhancement of photoresponse of more than a factor of 2 when measured from this junction. While it takes only 600 s to obtain such a pronounced increase in photoresponse, it persists for hours, indicating the feasibility of photovoltaic device performance control. The effect is ascribed to a charge injection-induced increase in minority carrier (hole) diffusion length (resulting in improved collection of photogenerated non-equilibrium carriers) in n-type β -Ga₂O₃ epitaxial layers due to trapping of injected charge (holes) on deep meta-stable levels in the material and the subsequent blocking of non-equilibrium carrier recombination through these levels. Suppressed recombination leads to increased non-equilibrium carrier lifetime, in turn determining a longer diffusion length and being the root-cause of the effect of charge injection.

Keywords: gallium oxide; spectral photoresponse; minority carriers



Citation: Schulte, A.; Modak, S.; Landa, Y.; Atman, A.; Li, J.-S.; Chiang, C.-C.; Ren, F.; Pearton, S.J.; Chernyak, L. Impact of Solid-State Charge Injection on Spectral Photoresponse of NiO/Ga₂O₃ p–n Heterojunction. *Condens. Matter* **2023**, *8*, 106. <https://doi.org/10.3390/condmat8040106>

Academic Editors: Amador Pérez Tomás, Ekaterine Chikoidze and Mike Jennings

Received: 26 October 2023

Revised: 22 November 2023

Accepted: 29 November 2023

Published: 2 December 2023



Copyright: © 2023 by the authors. Licensee MDPI, Basel, Switzerland. This article is an open access article distributed under the terms and conditions of the Creative Commons Attribution (CC BY) license (<https://creativecommons.org/licenses/by/4.0/>).

1. Introduction

Solar-blind photodetectors [1–4] are insensitive to infrared, visible, and near-UV light but respond to ultraviolet radiation with wavelengths below about 300 nm. These detectors are critical for a variety of applications, including the following:

- **Flame detection:** Solar-blind photodetectors can be used to detect flames, which emit UV light, even in the presence of sunlight or other visible light sources. This makes them useful for fire safety applications, such as in industrial plants and aircraft.
- **Missile launch detection:** Solar-blind photodetectors can be used to detect missile launches, which also emit UV light. This makes them useful for military and security applications.
- **Astronomical observation:** Solar-blind photodetectors can be used to observe astronomical objects in the UV spectrum, which is not possible with traditional optical telescopes.
- **Ozone layer monitoring:** Solar-blind photodetectors can be used to monitor the ozone layer, which absorbs UV light. This information can be used to track the depletion of the ozone layer and to predict the effects of climate change.

Solar-blind photodevices are typically made from semiconductors with a wide band gap. This means that only high-energy UV photons can be absorbed and generate a photocurrent.

Modern aircrafts need to be equipped with warning sensors operating in the ultraviolet (UV) part of the spectrum, especially in the ultraviolet-C (UVC) region spanning from 200 to 280 nm wavelength because the UVC is completely absorbed by the atmospheric ozone layer; therefore, only a UVC source of interest in the atmosphere below the ozone layer can be detected with solar-blind sensors [1–4]. The low false-alarm rate of the UV sensors is due to absence of background radiation, especially in the UVC region.

An emerging semiconductor with a direct bandgap of 4.6–4.9 eV, β -Ga₂O₃, has become an attractive candidate for sensing applications in the UVC region primarily due to its ultra-wide bandgap and superior radiation stability (due to wider bandgap) over GaN [1–8]. A drawback of Ga₂O₃ is the absence of robust p-type doping. All the potential acceptor dopants have large ionization energies and are not significantly ionized at room temperature. This has led to the use of p-type oxides, principally polycrystalline NiO, to form p–n heterojunctions with n-type Ga₂O₃ [9–17]. The forward current transport mechanism in such junctions is typically recombination under low-bias and trap-assisted tunneling under higher bias [13,18–22]. Conductivity modulation has been demonstrated during switching in these heterojunctions [23].

It has been previously shown that in p-type GaN and ZnO, electron beam or solid-state injection, using forward bias of p–n junctions, results in a significant increase in the minority carrier diffusion length [24–26]. Similar effects have recently been observed in n-type and highly resistive p-type Ga₂O₃ subjected to low-energy electron beam injection in scanning electron microscopes [27,28]. Diffusion length increase translates into experimentally demonstrated superior photovoltaic detector performance for GaN [29] and ZnO [30], with evidence of a similar effect for β -Ga₂O₃. However, the effect of electrical injection of carriers has not been demonstrated in this material because of the lack of p-type doping capability.

This work demonstrates the impact of forward bias charge injection on photoresponse in NiO/Ga₂O₃ p–n heterojunctions at room temperature. The results, which are summarized below, present the proof of concept and pave the way towards device performance control in Ga₂O₃ solar-blind UV photodetectors.

2. Experimental Section

The schematic for the vertical p–n NiO/Ga₂O₃ heterojunction is shown in Figure 1. Ga₂O₃ substrates—2-inch diameter, (001) orientation, Sn-doped (majority electron concentration $\sim 2 \times 10^{18} \text{ cm}^{-3}$)—were purchased from Novel Crystal Technology, Japan (<https://www.novelcrystal.co.jp/eng/>, accessed on 28 November 2023). For the substrates, X-ray diffraction revealed the full width at half maximum (FWHM) to be 150 arc sec in both [010] and [102] directions. Lightly doped with Si (majority electron concentration $\sim 2 \times 10^{16} \text{ cm}^{-3}$), 10- μm -thick gallium oxide drift layers were grown over the substrates via halide vapor phase epitaxy (HVPE). Prior to drift layer growth, the substrate was solvent-cleaned and heated to the growth temperature under Ar gas flow. Prior to nickel oxide deposition over the drift layer (cf. Figure 1), the surface was treated via UV/Ozone cleaning. The NiO bilayer was deposited via rf (13.56 MHz) magnetron sputtering at a working pressure of 3 mTorr [31]. The NiO bilayer consisted of a 10-nm layer with hole concentration $p = 3.0 \times 10^{18} \text{ cm}^{-3}$, and a 10-nm layer with hole concentration $p = 2.6 \times 10^{19} \text{ cm}^{-3}$, which were optimized to provide high breakdown voltage and optimal current spreading, respectively. The hole concentration in the NiO bilayer was adjusted using the Ar/O₂ ratio. The structure was then annealed at 300 °C under O₂. All majority carrier concentrations were measured at room temperature using the Hall effect setup. Finally, a top contact of 20/80 nm Ni/Au (1000 μm diameter) was deposited onto the NiO bilayer. Ohmic contacts were made to the rear surface using a Ti/Au metal stack deposited via e-beam evaporation followed by annealing at 550 °C for 180 s under N₂. The front surface was subjected to UV/Ozone exposure for 15 min to remove contamination prior to the metal deposition. More details on the vertical p–n NiO/Ga₂O₃ heterojunction fabrication can be found elsewhere [31].

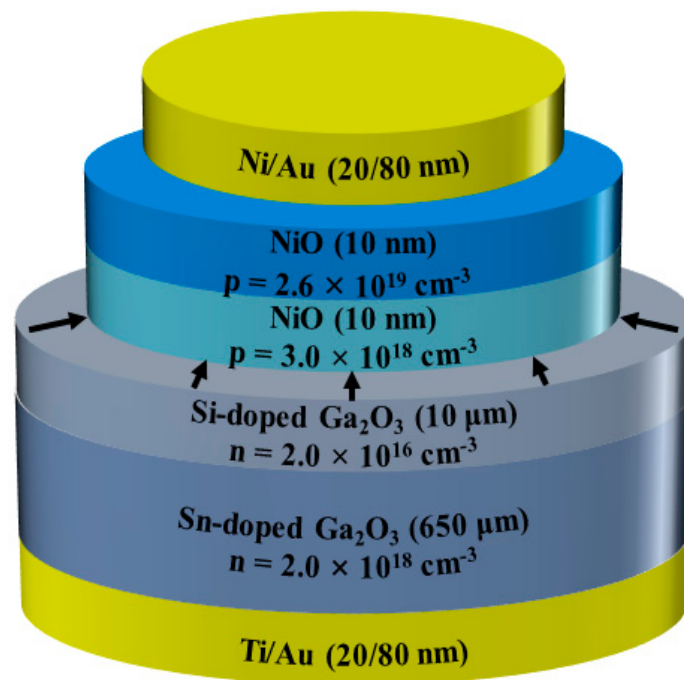


Figure 1. Schematics for the vertical p-n NiO/Ga₂O₃ heterojunction with the respective majority carrier concentrations and thicknesses. The centripetal arrows on the top plane of Si-doped 10-μm-thick n-type Ga₂O₃ layer show directions for a lateral diffusion and drift of light-induced non-equilibrium minority holes moving towards the depletion layer, which extends by ~180 nm beyond the p-niO/n-Ga₂O₃ interface.

The heterojunction shows the rectification of more than 5 orders of magnitude from 2 V forward to 10 V reverse bias, as shown in Figure 2a,b. The forward turn-on voltage for the junction is ~1.9 V (cf. Figure 2b) with on-resistance of 8 mΩ.cm⁻² [31]. The turn-on voltage is determined by band alignment between the two materials, as reported previously [13]. The band diagram for the NiO/Ga₂O₃ heterojunction, as a function of NiO postdeposition annealing temperature, is shown in Figure 3 [12].

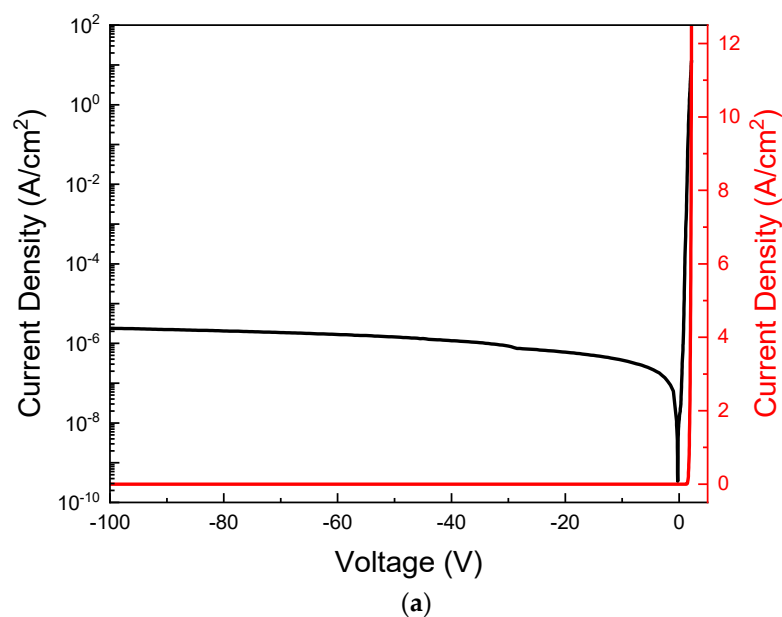


Figure 2. Cont.

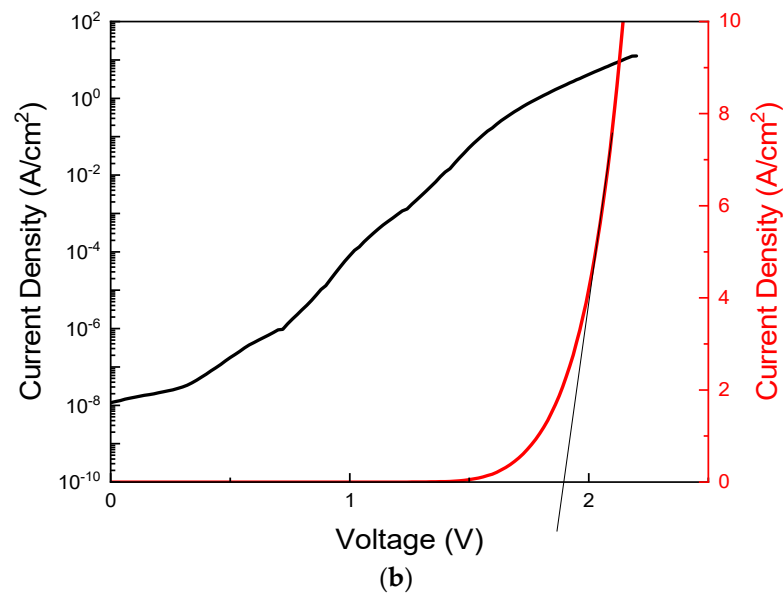


Figure 2. (a) Room temperature forward and reverse I-V (Current-Voltage) curves (linear and logarithmic scales) from the NiO/Ga₂O₃ p-n heterojunction shown in Figure 1. (b) Forward branch of the I-V curve shown in Figure 2 (a linear and logarithmic scale). The value for forward turn-on voltage of ~1.9 V is obtained via the intersection of the dashed black line, tangential to the I-V curve, with the voltage axis.

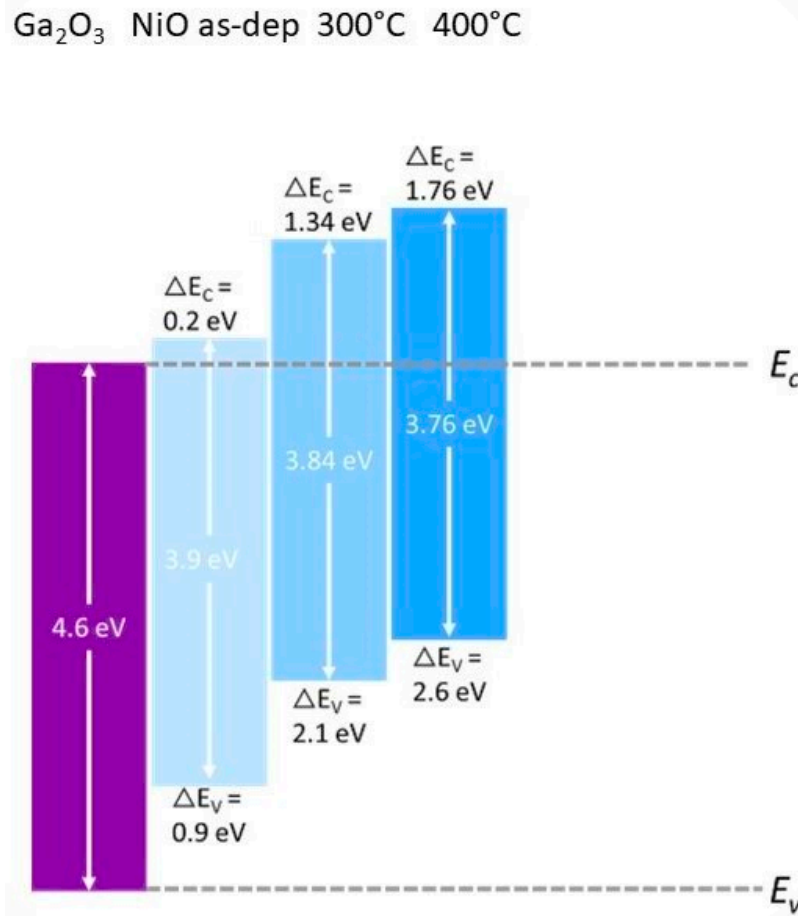


Figure 3. Band diagram for the NiO/Ga₂O₃ heterostructure as a function of NiO postdeposition annealing temperature (after ref. [12]).

Under forward bias, the depletion layer collapses, and holes diffuse into the Ga₂O₃. Drift is the dominating carrier transport under reverse bias due to the electric field. Diffusion is more important in the neutral region. There is a slight (0.2 V) offset in the I–V curve due to residual charges on the diode [32]. The I–V curve, in this case, shows a slightly different offset when the voltage swings from different directions.

The dominant carrier transport mechanism in the bipolar heterojunction diodes (HJDs) is trap-assisted tunneling [32]. In this work, the device under test exhibits a dominant carrier transport mechanism in the low-forward-bias regime, with minority carrier diffusion also being present, especially at higher forward bias. Because the doping level for the p-niO layer in Figure 1 is two orders of magnitude than that of n-Ga₂O₃, the heterojunction can be treated as a one-sided abrupt junction. Therefore, the lateral and vertical extension, d , of the depletion layer at the p⁺-NiO/n-Ga₂O₃ interface can be calculated as $d = [2\epsilon\epsilon_0(V_{bi} - V)/(qN_B)]^{0.5}$, where ϵ_0 stands for permittivity in vacuum; ϵ is Ga₂O₃ dielectric constant; V_{bi} is built-in potential; V is applied external bias; q is charge of electron; and N_B is bulk 10- μ m-thick n-type Si:Ga₂O₃ doping level (cf. Figure 1). Using the values presented for a similar calculation in ref. [27] resulted in $d \sim 180$ nm under zero bias. The maximum electric field strength at the p-niO/n-Ga₂O₃ interface was estimated at 0.8 MV.cm⁻¹, well below the maximum breakdown field of ~ 8 MV.cm⁻¹ [33].

The I–V curves of the p⁺-NiO/n-Ga₂O₃ heterojunction, presented in Figure 2a,b, were measured using a Keithley 2400 Source Meter. The measurements were carried out at room temperature. The same instrument was employed to drive a forward current of 100 μ A through the structure in Figure 1 for the total duration of 900 s, corresponding to the maximum charge of 90 mC. The forward current resulted in hole injection from p-niO to n-Ga₂O₃ layers and led to the results presented in the following section of this paper.

Room temperature spectral photoresponse was measured at zero bias in the 200–300 nm spectral range using a tunable light source, comprising a stabilized deuterium UV lamp (SLS204) coupled with a Horiba Triax 320 spectrometer. The latter is equipped with a grating with 150 grooves/mm blazed at 500 nm. The output beam of the monochromatic light was focused in the shape of rectangle (fully covering the whole top contact and extending to the opposite sides of it (cf. Figure 1)) and modulated at 95 Hz frequency. The induced photoresponse signal, measured at zero bias, was amplified using an Ithaco 393 lock-in amplifier, digitized with a Keithley 2000 digital multimeter, and recorded using homemade software. The spectra were measured prior to forward bias charge injection, followed by the measurements after 300, 600, and 900 s of bias.

3. Results and Discussion

The photoresponse from the structure in Figure 1 is presented in Figure 4 as a function of forward bias duration. All spectra exhibit shoulders at about 255 nm, corresponding to the direct band-to-band transition in β -gallium oxide [1–3,34]. The maxima for all spectra are observed between 230 and 240 nm and likely correspond to the excitonic absorption. These maxima (peaks), taken at the corresponding wavelength within the above-referenced range, are used in the future analysis. Similar photoresponse peaks were recently observed between 5.0 and 5.2 eV (238–248 nm wavelength range) in ref. [35], consistent with the band structure of the monoclinic Ga₂O₃ [34].

An increase of more than a factor of 2 in peak photoresponse was observed in Figure 4 while injecting the total charge of 60 mC for 600 s. Forward bias was continued for the total time of 900 s; however, the peak photosignal showed virtually no increase between 600 and 900 s (cf. Figure 5 below), thus indicating saturation for the effect of interest. Note that the slight change in the spectral shape in Figure 4, observed after 300 s of charge injection, is not very clear at this point, but we could speculate that it is related to the interplay between different excitonic absorption levels.

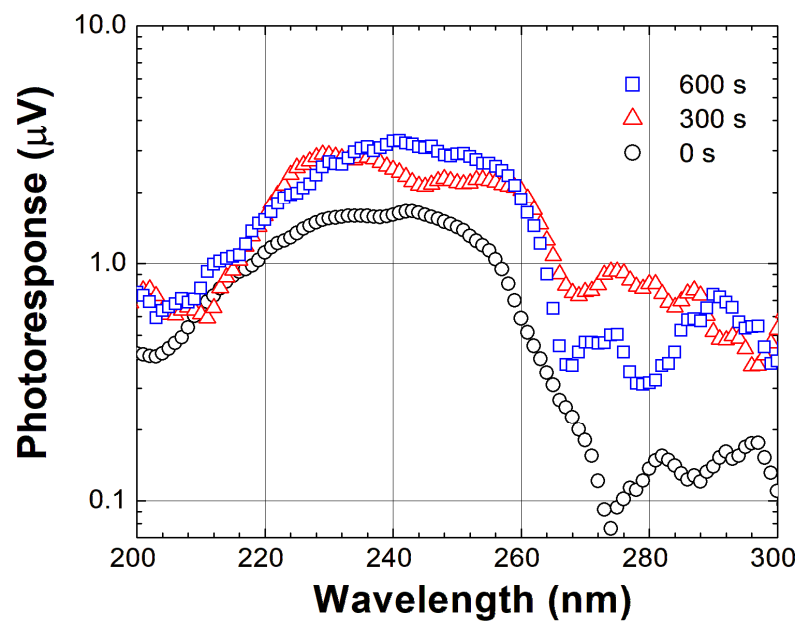


Figure 4. Zero-bias spectral photoresponse (in log scale) for the vertical p-n NiO/Ga₂O₃ heterojunction in Figure 1 as a function of forward bias hole injection duration. A total of 100 μ A was driven for the total duration of 600 s.

Ref. [27] reports detailed studies of charge injection-induced effects in n-type β -Ga₂O₃ subjected to low-energy (10 kV) electron beam irradiation in situ in a scanning electron microscope (SEM), which resulted in $\times 4$ increase in minority carrier (holes) diffusion length in the material at room temperature. Elongation of the diffusion length (L), measured using the electron beam-induced current (EBIC) technique in the region of charge-injection, was accompanied by a simultaneous decrease in cathodoluminescence (CL) intensity from the same region, which confirms the suppression of radiative recombination with increasing duration of charge injection. Because L is proportional to the square root of non-equilibrium carrier lifetime, τ , and CL intensity is proportional to τ^{-1} , both effects (L elongation and CL intensity decrease) were attributed to a lifetime increase in non-equilibrium carriers in the conduction and valence bands. Variable temperature EBIC measurements revealed a charge trap with the activation energy of 74 meV, which was responsible for the phenomena under investigation.

The experimental results, observed in Figure 4 of this article, as well as previously obtained results for GaN and ZnO structures [24–26,29,30], suggest the following:

1. Charge injection from the electron beam of SEM and forward bias injection, reported in this work, demonstrate similarities in terms of their impact on minority carrier diffusion length in gallium oxide. As was already mentioned above, forward bias application to the NiO/Ga₂O₃ p–n junction results in a decrease in the potential barrier (~ 1.03 V for V_{bi} [27]) at the interface of two semiconducting layers. As a result, the holes from p-niO are injected into n-Ga₂O₃ and likely become captured by meta-stable traps. Although the exact energetic location for these possible traps is yet unknown, ref. [32] recently reported a trapping level for holes in n-type Ga₂O₃ located 140 meV above the top of the valence band. This level was revealed via the deep level transient spectroscopy (DLTS) technique while studying hole injection via trap-assisted tunneling from p⁺-NiO into n-Ga₂O₃ under forward bias. Capturing injected charge carriers on meta-stable energetic levels prevents the recombination of light-induced non-equilibrium carriers in n-type gallium oxide through these levels. As a result, the non-equilibrium carriers remain in the respective valence and conduction bands of gallium oxide for longer periods, in turn leading to larger carrier lifetime, τ , and therefore longer diffusion length, L .

2. Although L was not directly measured for the structure shown in Figure 1 and studied in the experiments reported here, it is logical to assume that forward bias charge injection leads to an increase in minority hole diffusion length in the 10- μm -thick n-type Ga_2O_3 epitaxial layer in agreement with the mechanism described above and in ref. [29]. Because the concentration of majority carriers in n- Ga_2O_3 is two orders of magnitude lower than that of p-niO, the built-in electric field, employed for non-equilibrium carrier charge separation, is mostly localized in the 10- μm -thick n-type gallium oxide epitaxial layer (extends ~ 180 nm from the NiO/ Ga_2O_3 interface into 10 μm -thick n-Gallium Oxide [27]). Therefore, the diffusion length for minority holes in this layer are of primary importance.
3. According to ref. [36], which studied the absorption of UV radiation (at 250 nm) in the NiO/ Ga_2O_3 heterojunction, more than 80% of the light, shining vertically on the Ni/Au/NiO stack (cf. Figure 1), is absorbed and therefore does not reach the underlying 10- μm -thick n-type gallium oxide epitaxial layer. As a result, the only portion of 10- μm -thick Si-doped n- Ga_2O_3 , which is not covered by the above Ni/Au contact and NiO bilayer, contributes to the photoresponse. Therefore, the collection of non-equilibrium photoexcited carriers in n- Ga_2O_3 is lateral, as shown by the centripetal arrows in Figure 1, meaning that the non-equilibrium minority carriers (holes) are mostly swept by the vertical portion of the NiO/ Ga_2O_3 space charge region, which extends laterally (~ 180 nm) beyond the heterojunction interface.
4. The minority hole diffusion length, L , measured at room temperature in ref. [27] for n-type Ga_2O_3 using the electron beam-induced current (EBIC) technique, was reported at ~ 400 nm prior to electron beam injection. It is generally accepted that light-excited (due to illumination) non-equilibrium carriers, generated within $2L$ distance from the space-charge region (depletion region), are capable of diffusing without recombination towards the p-n junction, where they are swept by its internal electric field, thus contributing to a photocurrent. Therefore, longer diffusion length due to forward bias charge injection leads to the collection of photogenerated carriers from a larger area of the structure presented in Figure 1, thus enhancing collection (by the p-n heterojunction built-in field) efficiency for minority carriers (holes), and therefore representing the main factor that contributes to larger photoresponse with the increasing duration of forward bias [35].
5. It should be noted that the structure in Figure 1 is not optimized as a photodetecting device. Therefore, instead of presenting device's figures of merit, the relative photoresponse increase is demonstrated in Figure 4, thus serving as the proof of concept. While the responsivity (A/V) dependence on the wavelength is more appropriate for optimized device, the data presented in Figure 4 correspond to the output signal of the lock-in amplifier used for the measurements. Accounting for the lock-in amplifier sensitivity and input impedance, the maximum photocurrent is estimated at several fractions of pA. Fabrication of optimized structures is under way, and they will be studied in future experiments. The figures of merit for the optimized NiO/ Ga_2O_3 hetero p-n junctions, used as photovoltaic detectors, are summarized in ref. [36].

The dynamics of photoresponse increase as a function of forward bias duration is presented in Figure 5. The peak photoresponse, taken from the data in Figure 4 as described above, exhibits a linear increase as a function of time (injected charge) before it saturates at around 900 s. The nature of linear increase is related to two factors:

1. The minority carrier diffusion length depends linearly on charge injection duration as was previously observed for GaN, ZnO, and Ga_2O_3 [24–28].
2. In the configuration of the structure under test, in which the charge collection occurs laterally (cf. Figure 1 and the discussion outlined above), the photoresponse depends linearly on L , as explained in ref. [37]. Therefore, the linear increase for the peak photoresponse with duration of charge injection is confirmed, rather than revealed (as it is known and expected for the lateral charge collection [37]), in Figure 5. The peak

photoresponse after 900 s of charge injection, though shown in Figure 5, is not used for the linear fit, due to a clear saturation.

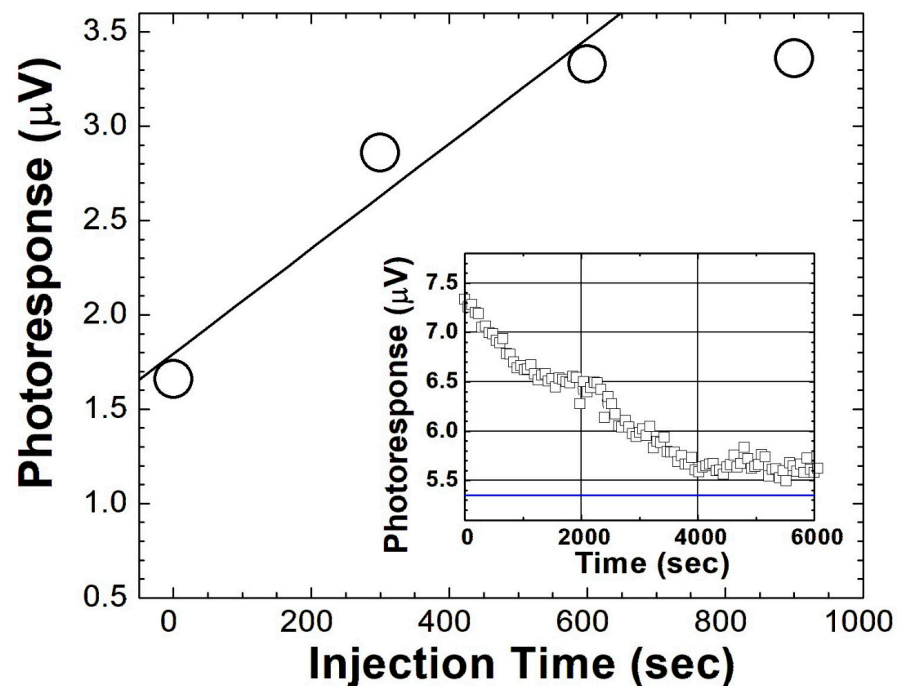


Figure 5. Dynamics of the peak photoresponse (taken for each spectrum in Figure 4 in the 230–240 nm range) enhancement (open circles) and the fit to the data before the saturation occurred at 900 s. The linear fit confirms the lateral charge collection as discussed in ref. [37].

The inset of Figure 5 demonstrates relaxation of the total photoresponse under polychromatic illumination followed saturation. It is not surprising that the amplitude for the signal in the inset of Figure 5 is larger than that in Figures 4 and 5, as the latter ones show a spectral dependence for the photoresponse. It is critical to emphasize that while it takes only 600 s to induce a more than a factor-of-2 increase in the peak photoresponse, it takes much longer (up to 6000 s) for the signal to decay to the baseline. This serves as a proof of the metastable nature of traps involved in the phenomenon of charge injection.

Inset: Dynamics of polychromatic photoresponse relaxation after saturation following forward bias injection. The blue line shows a polychromatic photoresponse from the structure before forward bias injection.

4. Summary

In summary, the effect of charge injection under forward bias was employed for improvement of the photoresponse from the NiO/ β -Ga₂O₃ p–n heterojunction. The charging of the metastable point defect levels in β -Ga₂O₃ is believed to be responsible for the phenomenon of interest. Because it only takes 600 s to induce an enhanced photoresponse, and because its slow decay occurs over hours, the effect has practical implications for the enhancement of detector performance. Combined with electronic circuitry for photosignal monitoring and periodic charge injection, once necessary, a new generation of higher efficiency photovoltaic devices could be fabricated. The advantage of the proposed method is that it does not involve costly technological modifications of the structure but is a purely electrical “athermal” approach, based on defect engineering. There is still much to be optimized in terms of device design, reliability, operational stability, and manufacturability, as detailed in the literature [38–56].

Author Contributions: Conceptualization, L.C.; methodology, S.M. and A.S.; software, A.S.; validation, L.C. and S.M.; formal analysis, A.S., L.C. and S.M.; investigation, Y.L., A.A., J.-S.L. and C.-C.C.; writing—original draft preparation, L.C. and J.-S.L.; writing—review and editing, L.C. and S.J.P.; supervision, A.S., L.C., F.R. and S.J.P.; project administration, A.S., L.C., F.R. and S.J.P.; funding acquisition, A.S., L.C., F.R. and S.J.P. All authors have read and agreed to the published version of the manuscript.

Funding: This research was supported, in part, by the US–Israel Binational Science Foundation (awards # 2022056 and # 2022779), the National Science Foundation (ECCS #2310285), and the NATO (G5748). The research at UF was performed as part of the Interaction of Ionizing Radiation with Matter University Research Alliance (IIRM-URA), sponsored by the Department of the Defense Defense Threat Reduction Agency under the award HDTRA1-20-2-0002. The content of the information does not necessarily reflect the position or the policy of the federal government, and no official endorsement should be inferred.

Data Availability Statement: The data presented in this paper are available from the corresponding author upon reasonable request.

Conflicts of Interest: The authors declare no conflict of interest.

References

1. Kalra, A.; Ul Muazzam, U.; Muralidharan, R.; Raghavan, S.; Nath, D.N. The road ahead for ultrawide bandgap solar-blind UV photodetectors. *J. Appl. Phys.* **2022**, *131*, 150901. [[CrossRef](#)]
2. Xie, C.; Lu, X.T.; Tong, X.W.; Zhang, Z.X.; Liang, F.X.; Liang, L.; Luo, L.B.; Wu, Y.C. Recent progress in solar-blind deep-ultraviolet photodetectors based on inorganic ultrawide bandgap semiconductors. *Adv. Funct. Mater.* **2019**, *29*, 1806006. [[CrossRef](#)]
3. Kaur, D.; Kumar, M. A Strategic Review on Gallium Oxide Based Deep-Ultraviolet Photodetectors: Recent Progress and Future Prospects. *Adv. Opt. Mater.* **2021**, *9*, 2002160. [[CrossRef](#)]
4. Xu, J.; Zheng, W.; Huang, F. Gallium oxide solar-blind ultraviolet photodetectors: A review. *J. Mater. Chem. C* **2019**, *7*, 8753. [[CrossRef](#)]
5. Flack, T.J.; Pushpakaran, B.N.; Bayne, S.B. GaN technology for power electronic applications: A review. *J. Electron. Mater.* **2016**, *45*, 2673. [[CrossRef](#)]
6. Ionascut-Nedelcescu, A.; Carlone, C.; Houdayer, A.; von Bardeleben, H.J.; Cantin, J.-L.; Raymond, S. Radiation hardness of gallium nitride. *IEEE Trans. Nucl. Sci.* **2002**, *49*, 2733. [[CrossRef](#)]
7. Onoda, S.; Hasuike, A.; Nabeshima, Y.; Sasaki, H.; Yajima, K.; Sato, S.I.; Ohshima, T. Enhanced charge collection by single ion strike in AlGaIn/GaN HEMTs. *IEEE Trans. Nucl. Sci.* **2013**, *60*, 4446. [[CrossRef](#)]
8. Nakamura, S.; Mukai, T.; Senoh, M. High-power GaN pn junction blue-light-emitting diodes. *Jpn. J. Appl. Phys.* **1991**, *30*, L1998. [[CrossRef](#)]
9. Kokubun, Y.; Kubo, S.; Nakagomi, S. All-oxide p–n heterojunction diodes comprising p-type NiO and n-type β -Ga₂O₃. *Appl. Phys. Express* **2016**, *9*, 091101. [[CrossRef](#)]
10. Deng, Y.; Yang, Z.; Xu, T.; Jiang, H.; Ng, K.W.; Liao, C.; Su, D.; Pei, Y.; Chen, Z.; Wang, G.; et al. Band alignment and electrical properties of NiO/ β -Ga₂O₃ heterojunctions with different β -Ga₂O₃ orientations. *Appl. Surf. Sci.* **2023**, *622*, 156917. [[CrossRef](#)]
11. Pintor-Monroy, M.I.; Barrera, D.; Murillo-Borjas, B.L.; Ochoa-Estrella, F.J.; Hsu, J.W.P.; Quevedo-Lopez, M.A. Tunable Electrical and Optical Properties of Nickel Oxide (NiO_x) Thin Films for Fully Transparent NiO_x-Ga₂O₃ p–n Junction Diodes. *ACS Appl. Mater. Interfaces* **2018**, *10*, 38159. [[CrossRef](#)]
12. Xia, X.; Li, J.-S.; Chiang, C.-C.; Yoo, T.J.; Ren, F.; Kim, H.; Pearton, S.J. Annealing temperature dependence of band alignment of NiO/ β -Ga₂O₃. *J. Phys. D Appl. Phys.* **2022**, *55*, 385105. [[CrossRef](#)]
13. Gong, H.; Chen, X.; Xu, Y.; Chen, Y.; Ren, F.; Liu, B.; Gu, S.; Zhang, R.; Ye, J. Band Alignment and Interface Recombination in NiO/ β -Ga₂O₃ Type-II pn Heterojunctions. *IEEE Trans. Electron Device* **2020**, *67*, 3341. [[CrossRef](#)]
14. Sharma, S.; Zeng, K.; Saha, S.; Singiseti, U. Field-Plated Lateral Ga₂O₃ MOSFETs With Polymer Passivation and 8.03 kV Breakdown Voltage. *IEEE Electron Device Lett.* **2020**, *41*, 836. [[CrossRef](#)]
15. Zhang, J.; Dong, P.; Dang, K.; Zhang, Y.; Yan, Q.; Xiang, H.; Su, J.; Liu, Z.; Si, M.; Gao, J.; et al. Ultra-wide bandgap semiconductor Ga₂O₃ power diodes. *Nat. Commun.* **2022**, *13*, 3900. [[CrossRef](#)] [[PubMed](#)]
16. Dong, P.; Zhang, J.; Yan, Q.; Liu, Z.; Ma, P.; Zhou, H.; Hao, Y. 6 kV/3.4 m Ω ·cm² Vertical β -Ga₂O₃ Schottky Barrier Diode With BV²/R_{on,sp} Performance Exceeding 1-D Unipolar Limit of GaN and SiC. *IEEE Electron Device Lett.* **2022**, *43*, 765. [[CrossRef](#)]
17. Lv, Y.; Wang, Y.; Fu, X.; Dun, S.; Sun, Z.; Liu, H.; Zhou, X.; Song, X.; Dang, K.; Liang, S.; et al. Demonstration of β -Ga₂O₃ Junction Barrier Schottky Diodes with a Baliga's Figure of Merit of 0.85 GW/cm² or a 5A/700 V Handling Capabilities. *IEEE Trans. Power Electron.* **2021**, *36*, 6179. [[CrossRef](#)]
18. Liao, C.; Lu, X.; Xu, T.; Fang, P.; Deng, Y.; Luo, H.; Wu, Z.; Chen, Z.; Liang, J.; Pei, Y.; et al. Optimization of NiO/ β -Ga₂O₃ Heterojunction Diodes for High-Power Application. *IEEE Trans. Electron Device* **2022**, *69*, 5722. [[CrossRef](#)]

19. Xiao, M.; Wang, B.; Liu, J.; Zhang, R.; Zhang, Z.; Ding, C.; Lu, S.; Sasaki, K.; Lu, G.-Q.; Buttay, C.; et al. Packaged Ga₂O₃ Schottky Rectifiers with Over 60-A Surge Current Capability. *IEEE Trans. Power Electron.* **2021**, *36*, 8565. [[CrossRef](#)]
20. Lu, X.; Zhou, X.; Jiang, H.; Ng, K.W.; Chen, Z.; Pei, Y.; Lau, K.M.; Wang, G. 1-kV Sputtered p-NiO/n-Ga₂O₃ Heterojunction Diodes with an Ultra-Low Leakage Current Below 1 μA/cm². *IEEE Electron Device Lett.* **2020**, *41*, 449. [[CrossRef](#)]
21. Wang, C.; Gong, H.; Lei, W.; Cai, Y.; Hu, Z.; Xu, S.; Liu, Z.; Feng, Q.; Zhou, H.; Ye, J.; et al. Demonstration of the p-NiO_x/n-Ga₂O₃ Heterojunction Gate FETs and Diodes With BV²/R_{on,sp} Figures of Merit of 0.39 GW/cm² and 1.38 GW/cm². *IEEE Electron Device Lett.* **2021**, *42*, 485. [[CrossRef](#)]
22. Yan, Q.; Gong, H.; Zhang, J.; Ye, J.; Zhou, H.; Liu, Z.; Xu, S.; Wang, C.; Hu, Z.; Feng, Q.; et al. β-Ga₂O₃ hetero-junction barrier Schottky diode with reverse leakage current modulation and BV²/R_{on,sp} value of 0.93 GW/cm². *Appl. Phys. Lett.* **2021**, *118*, 122102. [[CrossRef](#)]
23. Zhou, F.; Gong, H.; Xiao, M.; Ma, Y.; Wang, Z.; Yu, X.; Li, L.; Fu, L.; Tan, H.H.; Yang, Y.; et al. An avalanche-and-surge robust ultrawide-bandgap heterojunction for power electronics. *Nat. Commun.* **2023**, *14*, 4459. [[CrossRef](#)]
24. Chernyak, L.; Osinsky, A.; Fuflyigin, V.; Schubert, E.F. Electron beam-induced increase of electron diffusion length in p-type GaN and AlGa_N/Ga_N superlattices. *Appl. Phys. Lett.* **2000**, *77*, 875. [[CrossRef](#)]
25. Chernyak, L.; Nootz, G.; Osinsky, A. Enhancement of minority carrier transport in forward biased GaN pn junction. *Electron. Lett.* **2001**, *37*, 922. [[CrossRef](#)]
26. Lopatiuk-Tirpak, O.; Chernyak, L.; Xiu, F.X.; Liu, J.L.; Jang, S.; Ren, F.; Pearton, S.J.; Gartsman, K.; Feldman, Y.; Osinsky, A.; et al. Studies of minority carrier diffusion length increase in p-type ZnO:Sb. *J. Appl. Phys.* **2006**, *100*, 086101. [[CrossRef](#)]
27. Modak, S.; Lee, J.; Chernyak, L.; Yang, J.; Ren, F.; Pearton, S.J.; Khodorov, S.; Lubomirsky, I. Electron injection-induced effects in Si-doped β-Ga₂O₃. *AIP Adv.* **2019**, *9*, 015127. [[CrossRef](#)]
28. Modak, S.; Schulte, A.; Sartel, C.; Sallet, V.; Dumont, Y.; Chikoidze, E.; Xia, X.; Ren, F.; Pearton, S.J.; Ruzin, A.; et al. Impact of radiation and electron trapping on minority carrier transport in p-Ga₂O₃. *Appl. Phys. Lett.* **2022**, *120*, 233503. [[CrossRef](#)]
29. Chernyak, L.; Schulte, A.; Osinsky, A.; Graff, J.; Schubert, E.F. Influence of electron injection on performance of GaN photodetectors. *Appl. Phys. Lett.* **2002**, *80*, 926. [[CrossRef](#)]
30. Lopatiuk-Tirpak, O.; Chernyak, L.; Mandalapu, L.J.; Yang, Z.; Liu, J.L.; Gartsman, K.; Feldman, Y.; Dashevsky, Z. Influence of electron injection on the photoresponse of ZnO homojunction diodes. *Appl. Phys. Lett.* **2006**, *89*, 142114. [[CrossRef](#)]
31. Li, J.-S.; Xia, X.; Chiang, C.-C.; Hays, D.C.; Gila, B.P.; Craciun, V.; Ren, F.; Pearton, S.J. Deposition of sputtered NiO as a p-type layer for heterojunction diodes with Ga₂O₃. *J. Vac. Sci. Technol.* **2023**, *41*, 013405. [[CrossRef](#)]
32. Wang, Z.; Gong, H.; Meng, C.; Yu, X.; Sun, X.; Zhang, C.; Ji, X.; Ren, F.; Gu, S.; Zheng, Y.; et al. Majority and Minority Carrier Traps in NiO/β-Ga₂O₃ p⁺-n Heterojunction Diode. *IEEE Trans. Electron Devices* **2022**, *69*, 981. [[CrossRef](#)]
33. Wang, Z.P.; Gong, H.H.; Yu, X.X.; Hu, T.C.; Ji, X.L.; Ren, F.F.; Gu, S.L.; Zheng, Y.D.; Zhang, R.; Ye, J.D. Traps inhomogeneity induced conversion of Shockley–Read–Hall recombination in NiO/β-Ga₂O₃ p⁺-n heterojunction diodes. *Appl. Phys. Lett.* **2023**, *122*, 152102. [[CrossRef](#)]
34. Furthmüller, J.; Bedtke, F. Quasiparticle bands and spectra of Ga₂O₃ polymorphs. *Phys. Rev. B* **2016**, *93*, 115204. [[CrossRef](#)]
35. Verma, D. Measurement of Local Electric Fields and the Onset of Breakdown in Ultra-Wide Band Gap Semiconductor Devices Using Photocurrent Spectroscopy. Ph.D. Dissertation, Ohio State University, Columbus, OH, USA, 2023.
36. Vasquez, J.M.T.; Ashai, A.; Lu, Y.; Khandelwal, V.; Rajbhar, M.; Kumar, M.; Li, X.; Sarkar, B. A self-powered and broadband UV PIN photodiode employing a NiO layer and a β-Ga₂O₃ heterojunction. *J. Phys. D Appl. Phys.* **2023**, *56*, 065104. [[CrossRef](#)]
37. Holloway, H. Theory of lateral-collection photodiodes. *J. Appl. Phys.* **1978**, *49*, 4264. [[CrossRef](#)]
38. Ping, L.K.; Burhanuddin, D.D.; Mondal, A.K.; Menon, P.S.; Mohamed, M.A. Properties and perspectives of ultrawide bandgap Ga₂O₃ in optoelectronic applications. *Chin. J. Phys.* **2021**, *73*, 195. [[CrossRef](#)]
39. Wang, C.; Zhang, J.; Xu, S.; Zhang, C.; Feng, Q.; Zhang, Y.; Ning, J.; Zhao, S.; Zhou, H.; Hao, Y. Progress in state-of-the-art technologies of Ga₂O₃ devices. *J. Phys. D Appl. Phys.* **2021**, *54*, 243001. [[CrossRef](#)]
40. Sheeran, H.; Kumar, V.; Singh, R. A comprehensive review on recent developments in ohmic and Schottky contacts on Ga₂O₃ for device applications. *ACS Appl. Electron. Mater.* **2022**, *4*, 2589. [[CrossRef](#)]
41. Reese, S.B.; Remo, T.; Green, J.; Zakopane, A. How Much Will Gallium Oxide Power Electronics Cost? *Joule* **2019**, *3*, 903. [[CrossRef](#)]
42. Zhou, H.; Zhang, J.; Zhang, C.; Feng, Q.; Zhao, S.; Ma, P.; Hao, Y. A review of the most recent progresses of state-of-art gallium oxide power devices. *J. Semicond.* **2019**, *40*, 011803. [[CrossRef](#)]
43. Wang, B.; Xiao, M.; Spencer, J.; Qin, Y.; Sasaki, K.; Tadjer, M.J.; Zhang, Y. 2.5 kV Vertical Ga₂O₃ Schottky Rectifier with Graded Junction Termination Extension. *IEEE Electron Device Lett.* **2023**, *44*, 221. [[CrossRef](#)]
44. Liu, A.-C.; Hsieh, C.-H.; Langpoklakpam, C.; Singh, K.J.; Lee, W.-C.; Hsiao, Y.-K.; Horng, R.-H.; Kuo, H.-C.; Tu, C.-C. State-of-the-Art β-Ga₂O₃ Field-Effect Transistors for Power Electronics. *ACS Omega* **2022**, *7*, 36070. [[CrossRef](#)]
45. Guo, W.; Han, Z.; Zhao, X.; Xu, G.; Long, S. Large-area Ga₂O₃ Schottky barrier diode and its application in DC-DC converters. *J. Semicond.* **2023**, *44*, 072805. [[CrossRef](#)]
46. Wei, Y.; Peng, X.; Jiang, Z.; Sun, T.; Wei, J.; Yang, K.; Hao, L.; Luo, X. Low Reverse Conduction Loss β-Ga₂O₃ Vertical FinFET with an Integrated Fin Diode. *IEEE Trans. Electron Devices* **2023**, *70*, 3454. [[CrossRef](#)]
47. Hao, W.; Wu, F.; Li, W.; Xu, G.; Xie, X.; Zhou, K.; Guo, W.; Zhou, X.; He, Q.; Zhao, X.; et al. Improved Vertical β-Ga₂O₃ Schottky Barrier Diodes with Conductivity-Modulated p-NiO Junction Termination Extension. *IEEE Trans. Electron Devices* **2023**, *70*, 2129. [[CrossRef](#)]

48. Wu, F.; Wang, Y.; Jian, G.; Xu, G.; Zhou, X.; Guo, W.; Du, J.; Liu, Q.; Dun, S.; Yu, Z.; et al. Superior Performance β -Ga₂O₃ Junction Barrier Schottky Diodes Implementing p-NiO Heterojunction and Beveled Field Plate for Hybrid Cockcroft–Walton Voltage Multiplier. *IEEE Trans. Electron Devices* **2023**, *70*, 1199. [[CrossRef](#)]
49. Hao, W.; He, Q.; Zhou, K.; Xu, G.; Xiong, W.; Zhou, X.; Jian, G.; Chen, C.; Zhao, X.; Long, S. Low defect density and small I–V curve hysteresis in NiO/ β -Ga₂O₃ pn diode with a high PFOM of 0.65 GW/cm². *Appl. Phys. Lett.* **2021**, *118*, 043501. [[CrossRef](#)]
50. Yan, Q.; Gong, H.; Zhou, H.; Zhang, J.; Ye, J.; Liu, Z.; Wang, C.; Zheng, X.; Zhang, R.; Hao, Y. Low density of interface trap states and temperature dependence study of Ga₂O₃ Schottky barrier diode with p-NiO_x termination. *Appl. Phys. Lett.* **2022**, *120*, 092106. [[CrossRef](#)]
51. Zhou, F.; Gong, H.; Wang, Z.; Xu, W.; Yu, X.; Yang, Y.; Ren, F.-F.; Gu, S.; Zhang, R.; Zheng, Y.; et al. Over 1.8 GW/cm² beveled-mesa NiO/ β -Ga₂O₃ heterojunction diode with 800 V/10 A nanosecond switching capability. *Appl. Phys. Lett.* **2021**, *119*, 262103. [[CrossRef](#)]
52. Zhou, F.; Gong, H.; Xu, W.; Yu, X.; Xu, Y.; Yang, Y.; Ren, F.-F.; Gu, S.; Zheng, Y.; Zhang, R. 1.95-kV beveled-mesa NiO/ β -Ga₂O₃ heterojunction diode with 98.5% conversion efficiency and over million-times overvoltage ruggedness. *IEEE Trans. Power Electron.* **2021**, *37*, 1223. [[CrossRef](#)]
53. Chi, Z.; Asher, J.J.; Jennings, M.R.; Chikoidze, E.; Pérez-Tomás, A. Ga₂O₃ and related ultra-wide bandgap power semiconductor oxides: New energy electronics solutions for CO₂ emission mitigation. *Materials* **2022**, *15*, 1164. [[CrossRef](#)] [[PubMed](#)]
54. Gong, H.; Chen, X.; Xu, Y.; Ren, F.-F.; Gu, S.; Ye, J. A 1.86-kV double-layered NiO/ β -Ga₂O₃ vertical p–n heterojunction diode. *Appl. Phys. Lett.* **2020**, *117*, 022104. [[CrossRef](#)]
55. Gong, H.; Yu, X.; Xu, Y.; Chen, X.; Kuang, Y.; Lv, Y.; Yang, Y.; Ren, F.-F.; Feng, Z.; Gu, S.L.; et al. β -Ga₂O₃ vertical heterojunction barrier Schottky diodes terminated with p-NiO field limiting rings. *Appl. Phys. Lett.* **2021**, *118*, 202102. [[CrossRef](#)]
56. Gong, H.; Zhou, F.; Xu, W.; Yu, X.; Xu, Y.; Yang, Y.; Ren, F.-F.; Gu, S.; Zheng, Y.; Zhang, R. 1.37 kV/12 A NiO/ β -Ga₂O₃ heterojunction diode with nanosecond reverse recovery and rugged surge-current capability. *IEEE Trans. Power Electron.* **2021**, *36*, 12213. [[CrossRef](#)]

Disclaimer/Publisher’s Note: The statements, opinions and data contained in all publications are solely those of the individual author(s) and contributor(s) and not of MDPI and/or the editor(s). MDPI and/or the editor(s) disclaim responsibility for any injury to people or property resulting from any ideas, methods, instructions or products referred to in the content.